Development of Low-cost Sodium-Aqueous Polysulfide Hybrid Batteries

Martha M. Gross and Arumugam Manthiram*

Materials Science & Engineering Program and Texas Materials Institute
The University of Texas at Austin, Austin, Texas 78712, United States

ABSTRACT

There has been increasing interest in sodium-sulfur (Na-S) batteries as an option for low-cost grid-scale energy storage. However, traditional Na-S batteries operate at high temperatures, raising concerns about long-term maintenance costs and safety. On the other hand, room-temperature Na-S batteries have their own limitations, including Na dendrite formation, polysulfide shuttling, and low utilization of active material. To overcome these issues, we present here a novel low-cost room-temperature sodium-aqueous polysulfide (Na-APS) hybrid battery system with a Na-metal anode, Na^+-ion solid electrolyte separator, and an aqueous polysulfide catholyte. The solid electrolyte blocks Na dendrites and polysulfide shuttling while simultaneously protecting the reactive Na metal anode from the aqueous catholyte. The redox kinetics of the APS catholyte is improved with a rational development of a freestanding CuS-CNT catalytic electrode. The improvements with the Na-APS hybrid battery compared to the traditional Na-S battery systems are discussed. The Na-APS hybrid battery displays excellent performance under a 418 mA h g^{-1} of sulfur capacity-restricted cycling. The battery achieves an energy efficiency of 90% over 100 cycles at 0.5 mA cm^{-2} current density.

Keywords: sodium-sulfur batteries; hybrid batteries; solid electrolytes; aqueous polysulfides; electrochemistry

*Corresponding author:
manth@austin.utexas.edu (A. Manthiram)

1. Introduction

Interest in energy storage is becoming widespread as the world moves towards a sustainable future built on renewable energy generation. To date, energy storage systems beyond pumped hydro have lagged far behind in terms of both development and deployment [1-2]. To compete with traditional energy generation, such as fossil fuels and nuclear, energy storage for the electric grid must be ultra-low cost to be competitive [3-5]. The sodium-sulfur system has enjoyed renewed interest in this regard as it makes use of abundant, inexpensive materials. However, traditional sodium-sulfur batteries are operated at temperatures at around 300 °C, leading to concerns regarding their safety and reliability [6-9]. Furthermore, costs over the battery lifetime associated with parasitic losses to maintain battery temperature eat into the levelized cost of storage [10-11]. To improve the safety and reduce the cost, there has been strong interest in developing room-temperature sodium-sulfur batteries [12-13].

The development of room-temperature sodium-sulfur (RT Na-S) batteries is still hindered by a number of issues. As with lithium-sulfur batteries, elemental sulfur and its final discharge products sodium disulfide (Na_2S_2) and sodium sulfide (Na_2S) are inherently highly insulating, requiring a high amount of electrochemically inactive conductive materials, which effectively lowers the system energy density [14-15]. The high solubility of intermediate sodium polysulfides in organic electrolytes and the resultant polysulfide shuttling also remain an issue for RT Na-S batteries [16-19]. The free migration of intermediate polysulfides and their reaction with the sodium anode ultimately causes a loss of active material, a lowered energy density, and a decreased cycle life. Furthermore, the Na-metal anode poses the risk of Na dendrite formation, resulting in internal battery shorting and a large safety hazard as a result [20-21]. There has been interest in protecting the Na anode by means of a solid-electrolyte separator to block Na dendrites and prevent

polysulfide shuttling. Until recently, however, commercially-available high-ionic conductivity solid electrolytes have been restricted solely to β" alumina, which is both air- and water-sensitive [10, 22]. Wenzel et al. demonstrated a RT Na-S battery with a β" alumina solid electrolyte and a simple ball-milled sulfur-carbon electrode that displayed an initial discharge capacity of 475 mA h g^{-1} and a capacity retention of 42% over 40 cycles [23]. Kim et al. also utilized a β" alumina solid electrolyte in a RT Na-S battery, demonstrating improved performance with a activated carbon-sulfur composite electrode and achieving an initial capacity of 855 mA h g^{-1} and a capacity retention of 61% over 104 cycles [24]. However, the capacity loss during cycling demonstrates that the use of a solid electrolyte does not fully solve the many issues associated with the sulfur cathode.

Recently, there have been significant development of several lithium and sodium hybrid battery systems in which an aqueous cathode is used, and the reactive lithium or sodium metal anode is protected by means of a solid electrolyte. This concept has been applied to hybrid lithium-air, sodium-air, and lithium-aqueous polysulfide batteries [25-28]. However, this concept has not been applied towards the development of a sodium-aqueous polysulfide batteries. We demonstrate here, for the first time, a sodium-aqueous polysulfide (Na-APS) hybrid battery. The Na-APS hybrid battery consists of a Na-metal anode in an organic electrolyte, a solid-electrolyte separator, and a fully liquid aqueous polysulfide catholyte (Fig. 1). The NASICON solid-electrolyte separator with a high ionic conductivity ($\sigma = \sim 1 \times 10^{-3}$ S cm^{-1}) protects the Na-metal anode from the aqueous catholyte and blocks Na dendrites from internal shorting and catastrophic battery failure. Furthermore, the use of a solid electrolyte allows independent optimization of the anolyte and catholyte and enables compositional tuning to achieve the desired properties. Additionally, the use

of a solid electrolyte completely eliminates crossover of polysulfides. As a result, the cathode of such a system can be optimized for fast redox kinetics, rather than confinement of the polysulfide.

The use of aqueous polysulfide has some distinct advantages over its nonaqueous counterpart. In a traditional sulfur cathode, discharge of the sulfur involves a solid-liquid transition from elemental cyclooctasulfur to Na_2S_8 and then liquid-liquid reactions between the high-order polysulfides (Na_2S_x $4 \leq x \leq 8$) followed by a liquid-solid transition from dissolved Na_2S_4 to solid Na_2S_3, Na_2S_2, or Na_2S and finally a solid-solid reaction between Na_2S_2 and Na_2S [13]. The solid-liquid and solid-solid reactions have particularly slow kinetics resulting in high overpotentials and low capacity retention. Furthermore, the solid-liquid-solid reactions and differing densities between sulfur and the final discharge product Na_2S cause the active material to undergo a substantial volume change, which must be accommodated by the electrode. In contrast, aqueous polysulfide is cycled entirely within the liquid regime, which allows for fast redox kinetics. Low-order polysulfides (Na_2S_x $1 \leq x \leq 4$) are fully soluble in water to very high concentrations, allowing for high system energy densities [29-30]. Cycling in the all-liquid regime of the lower order polysulfides avoids the liquid-solid transitions and their associated capacity loss, allowing for enhanced capacity retention. Restricting the capacity to prevent sulfur precipitation does lower the theoretical capacity from 1,675 mA h g^{-1} of sulfur to 1,256 mA h g^{-1}. However, this is still an extremely high capacity.

As aqueous polysulfides are confined by the solid electrolyte, there is no need to further confine the polysulfides at the electrode surface as is typically necessary in nonaqueous RT Na-S batteries. However, the redox kinetics of aqueous polysulfide are still sluggish and benefit from the use of a catalyst [31-32]. Transition-metal sulfides are typically favored as catalysts for their stability and high catalytic activity [33-35]. In nonaqueous systems, molybdenum disulfide (MoS_2)

is favored for its high adsorption of polysulfides, but in aqueous systems, cobalt sulfide (CoS) is favored for its high activity and stability [26, 36-39]. We have recently demonstrated high catalytic activity and stability with covellite phase copper sulfide (CuS) towards aqueous polysulfide as well [40]. In this work, we present the development of a freestanding electrode made of CuS hollow microtubes and carbon nanotubes (CNTs). The use of a freestanding electrode eliminates the use of binder materials, and the highly porous electrode allows the aqueous polysulfides to have a free access to the catalyst surface. We demonstrate excellent performance with the Na-APS hybrid system over 100 cycles, highlighting how the system differs from traditional RT Na-S batteries and the effect of CuS catalyst on battery rate performance.

2. Experimental

2.1 Synthesis of freestanding CuS-CNT electrodes

Copper sulfide (CuS) hollow microtubes were synthesized by a method described by Yao et al. [41], in which 2.4 mmol of cupric chloride ($CuCl_2$, 99%, Acros Organics) in 40 mL of deionized water was mixed with 2.4 mmol of thioacetamide (TAA, 99%, Chem-Impex International) in 30 mL of deionized water and allowed to react at room temperature for a few minutes. Once a yellow suspension was formed, the mixture was covered and transferred to a 60 °C oil bath for 24 h without stirring. The resulting black precipitate was recovered by vacuum filtration and dried overnight in a 50 °C vacuum oven. 56 mg of multi-wall carbon nanotubes (CNT, 95+%, NanoAmor)) + 15 mg of single-wall carbon nanotubes (CNT, 75%, TUBALL) were sonicated in ~ 65 mL of ethanol until fully suspended (~ 45 minutes). 24 mg of CuS was added to the mixed CNT suspension and stirred for 10 minutes. The mixture was then vacuum filtrated to form a freestanding electrode with a CuS loading of 1.7 mg cm^{-2}. The resulting freestanding CuS-

CNT electrode was dried overnight in a 50 °C vacuum oven. Freestanding CNT electrodes were also prepared in the same manner, without CuS microtubes.

2.2 Cell assembly

Na-APS hybrid batteries were assembled with a custom layered housing, as described in our previous work with lithium-air hybrid batteries and zinc-aqueous polysulfide batteries [42-43]. A schematic of the housing and cell assembly is shown in Fig. S1 in the supporting information, with further details of cell assembly. The batteries consisted of a Ni foam current collector, Na-metal chip (~ 100 mg, ACS reagent; dry, Sigma Aldrich), 1 M $NaClO_4$ (99+%, Acros Organics) in ethylene carbonate (EC, 99%, Sigma Aldrich) : propylene carbonate (PC, 99.5%, Acros Organics) (1:1 v/v) + 5 % fluoroethylene carbonate (FEC, BASF) additive anolyte (~ 1 mL), NASICON $Na_3Zr_2Si_2PO_{12}$ ceramic electrolyte (hand-polished to 0.5 mm thickness, 95% with ZrO_2 impurity, 4 to One Energy), aqueous polysulfide catholyte at the specified concentrations, freestanding CuS-CNT catalytic electrode, and 316 stainless steel mesh current collector unless otherwise noted. NASICON surface morphology can be seen in Fig. S2. Anodes were assembled in an argon-filled glovebox, before completing the battery assembly in a nitrogen-purged glovebag. Aqueous catholytes were prepared by mixing anhydrous sodium sulfide (Na_2S, 96%, Alfa Aesar) and elemental sulfur (S, 99.5%, Acros Organics) in a 1 : 3 molar ratio in a sodium hydroxide (NaOH, 97+%, Fisher Scientific) solution under nitrogen flow in a Schlenk line to form a nominal 0.25 M Na_2S_4 + NaOH solution. Catholytes containing 0.1 M NaOH and 1 M NaOH were tested.

2.3 Materials characterization and electrochemical measurements

The morphology and composition of freestanding CuS-CNT electrodes were analyzed, respectively, with an FEI Quanta field emission scanning electron microscope (SEM) equipped with a Bruker energy dispersive x-ray spectrometer (EDS). The phase of the electrode was determined with a Rigaku MiniFlex x-ray diffractometer (XRD). Cyclic voltammetry (CV) was performed on batteries with an Autolab PGSTAT302N potentiostat (Eco Chemie B.V.) at a scan rate of 0.1 mV s^{-1}. Batteries for CVs were assembled with 0.1 M Na_2S_4 + 1mM NaOH catholyte with catalyst-free CNT electrodes. Galvanostatic cycling was performed with an Arbin BT 2000 battery cycler. Rate testing was performed by charging and discharging a Na-APS cell for 20 minutes at each current density for 5 cycles. Results for the 5^{th} cycle at each current density is shown. Na-APS hybrid batteries for single discharge-charge cycle and for rate testing were assembled with 0.25 M Na_2S_4 + 1 M NaOH catholyte. Na-APS hybrid batteries for galvanostatic cycling were assembled with 0.25 M Na_2S_4 + 0.1 M NaOH unless otherwise noted.

3. Results and Discussion

3.1 Materials characterization

A schematic of the freestanding CuS-CNT electrode preparation can be seen in Fig. 2a. CuS hollow microtubes were synthesized by mixing equimolar amounts of cupric chloride ($CuCl_2$) and thioacetamide (TAA) [41] to form $Cu_3(TAA)_3Cl_3$ hexagonal prisms. After the prisms begin to form as indicated by the formation of a yellow precipitate, the mixture was transferred to a 60 °C oil bath and allowed to react for 24 h without stirring. The $Cu_3(TAA)_3Cl_3$ acts as a self-sacrificing template, on which spherical CuS nanoparticles grow from the surface. The CuS nanoparticles grow to form nanoflowers which aggregate to form a hollow microtube after fully cannibalizing

the $Cu_3(TAA)_3Cl_3$ self-sacrificing hexagonal prism template. A mixture of multi-wall CNTs and single-wall CNTs was fully suspended in ethanol by sonication and then the CuS microtubes were stirred into the CNT mixture. The CuS-CNT mixture was then vacuum-filtrated to form an electrode and dried overnight. Fig. 2b shows the morphology and composition of the freestanding CuS-CNT electrode as determined by scanning electron microscopy (SEM) and energy dispersive x-ray spectroscopy (EDS) mapping. Fig. 2c-e shows higher resolution SEM images of, respectively, the CuS microtube, the CuS nanoflowers, and the interwoven CNT. Fig. 2f confirms the electrode to consist of covellite phase CuS and CNT by X-ray diffraction (XRD), matching, respectively, JCPDS references 01-076-2321 and 75-1624. The CuS microtubes in the CuS-CNT electrode show excellent stability after cycling in a Na-APS hybrid battery for 100 cycles at 0.5 mA cm^{-2} current density, as shown in Fig. S3.

3.2 Electrochemical behavior

The electrochemical behavior and performance of the Na-APS hybrid battery was probed by cyclic voltammetry and galvanostatic cycling. The Na-APS cells assembled as described in the experimental section were investigated with cyclic voltammetry (CV), as shown in Fig. 3a-b. CVs were performed with Na-APS cells with dilute catholyte solutions (0.1 M Na_2S_4 + 1mM NaOH) and non-catalytic CNT electrodes to distinguish the individual redox peaks at a scan rate of 0.1 mV s^{-1}. This was due to the fact that redox peaks were not distinguishable in the CVs obtained with concentrated Na_2S_4 catholyte and CuS-CNT catalytic electrodes even at low scan rates like that shown in Fig. S4, as is typical for aqueous polysulfide catholytes [26, 30, 32, 43]. CVs undertaken in the voltage regime of traditional RT Na-S cells that use all-organic electrolytes immediately show the differences between them and the hybrid Na-APS cell. For RT Na-S

batteries, the organic electrolyte used allows for a very wide voltage stability window, permitting the discharge of sulfur to low voltages (1.2 V versus Na/Na^+). In the Na-APS hybrid battery, Fig. 3a shows that voltages below 1.8 V vs Na/Na^+ are outside the stability window of water, and the catholyte undergoes the hydrogen evolution reaction (HER). However, due to the much better redox kinetics of sodium polysulfide in water, the full discharge of Na_2S_4 to Na_2S occurs above the water splitting potential. Fig. 3b illustrates the CV between 1.8 and 2.8V, displaying a characteristic profile for aqueous polysulfide redox. These results indicate that the Na-APS hybrid battery shows remarkably low overpotentials associated with Na_2S_4 to Na_2S redox and should, therefore, exhibit a high energy density, but care must be taken not to ingress into the HER regime during cycling.

The Na-APS hybrid battery was further tested by performing a single deep cycle, in which a cell was discharged to the 1.8 V HER limit, then charged to an upper voltage limit of 2.9 V to fully precipitate sulfur at a current density of 0.5 mA cm^{-2} (Fig. 3c). The discharge step shows a narrow sloping voltage region until 2.1 V, then a long plateau region before the voltage drops off. This differs from our previous work with zinc-aqueous polysulfide batteries, in which only a single voltage plateau is observed on discharge [43]. Rudola et al. demonstrated with Na metal half-cells that the inclusion of EC in PC-based electrolytes introduces this voltage anomaly [44]. A separate Na-APS cell assembled with 1 M $NaClO_4$ in PC-only electrolyte does not show the initial sloping voltage region on discharge, as shown in Fig. 3d. This confirms that anolyte composition has some effect on the voltage profile of the Na-APS cell and may indicate its electrochemical participation during cycling.

The Na-APS hybrid battery performance was evaluated by galvanostatic cycling at different current densities, as shown in Fig. 4. Batteries were assembled with 1 M $NaClO_4$ in EC :

PC + 5% FEC anolyte, and 0.25 M Na_2S_4 + 0.1 M NaOH catholyte. Table S1 summarizes the current density, capacity, and energy density of the Na-APS hybrid batteries in the common units used in the reporting of hybrid batteries, sulfur batteries, and flow batteries. Aqueous polysulfide batteries are traditionally cycled between the Na_2S_4 and Na_2S_2 species to achieve good capacity retention, as demonstrated in polysulfide-bromine and polysulfide-air redox flow batteries [45-46]. Batteries that are deep discharged to Na_2S exhibit linear capacity loss [26, 43]. It was surmised by Demir-Cakan et al. that H_2S gas generation during polysulfide reduction is the main reason for this capacity loss [47]. For this work, Na-APS hybrid batteries were cycled with a capacity limit of 418 mA h g^{-1} of sulfur based on the theoretical capacity of the Na_2S_4 to Na_2S_2 redox reactions to ensure cycling above the redox of Na_2S and below the redox of solid sulfur. Fig. 4a-b displays the voltage profile, specific energy, and energy efficiency of a Na-APS hybrid battery cycled at 0.5 mA cm^{-2} current density. Despite only cycling one quarter of the capacity of sulfur, due to the low overpotential associated with the catalyzed aqueous polysulfide redox reactions and the corresponding high voltage of the battery, the Na-APS hybrid battery demonstrated an excellent average specific energy of 910 Wh kg^{-1} over 100 cycles. The voltage profile over that time shows a second plateau on charge and discharge. This is likely caused by the loss of active material during discharge to H_2S formation despite the capacity-limited cycling, which is then compensated for by overcharging the remaining Na_2S_2 to reach the 418 mA h g^{-1} charge capacity in the cycling schedule. Interestingly, the partial charge and discharge of solid sulfur appears to be relatively efficient in this system, and the energy efficiency of the battery remains steady during cycling. Over 100 cycles, the average energy efficiency was 90%.

Accelerated cycling of Na-APS hybrid batteries was also performed at 2 mA cm^{-2} current density with the capacity limits of 418 mA h g^{-1}. Voltage limits of 1.65 V and 2.8 V (versus

Na/Na^+) were also imposed to avoid water splitting. The lower voltage limit was tolerated due to the higher overpotential associated with HER at the high current density. As Fig. 4c shows, the first cycle of the Na-APS hybrid battery displayed two plateaus on discharge, and prematurely hit the voltage limit on charge due to a large overpotential. Subsequent cycles saw the first plateau turn into a sloped voltage feature seen previously in Fig. 3c and Fig. 4a. The overpotential decreased for 10 cycles until it became steady. This is reflected in the initially increasing energy efficiency of the battery, as shown in Fig. 4d. Overall, the Na-APS hybrid battery under a high current density exhibits remarkable stability. The capacity profile highlights that unlike at low current density, the Na-APS hybrid battery demonstrates no development of a second plateau at 2 mA cm^{-2} during cycling. The Na-APS hybrid battery is able to maintain a specific energy of 765 Wh kg^{-1} with energy efficiency of 70 % over 200 cycles. The effect of increasing the NaOH concentration in the catholyte in an effort to reduce H_2S gas generation was also tested, but it was shown to have a negligible effect on the Na-APS hybrid battery performance. Data for a Na-APS hybrid battery with 0.25 M Na_2S_4 + 1 M NaOH is shown in Fig. S5.

The rate capability of the Na-APS hybrid battery was also tested with and without the use of the CuS catalyst in the freestanding electrode to verify its catalytic activity. Rate testing was performed by discharging and charging the Na-APS hybrid batteries for 20 minutes at each current density. As can be seen in Fig. 5a-b, the rate performance of the Na-APS hybrid battery is substantially better when the CuS catalyst is used. Na-APS hybrid batteries with CuS-CNT electrodes achieved a power density of 5.2 mW cm^{-2}, while catalyst-free Na-APS hybrid batteries with CNT electrodes only achieved a power density of only 2.2 mW cm^{-2}. A comparison of the catalytic activity of CuS-CNT to traditional CuS and CoS catalytic electrodes is shown in Fig. S6. Closer analysis of the discharge profiles at each current density in the Na-APS hybrid battery with

CuS-CNT electrode shows that as the current density is increased, the voltage feature seen in Fig. 3d appears and becomes more pronounced. This is in good agreement with the work from Rudola et al. [44] that discussed the rate-dependence of the voltage feature in addition to its electrolyte dependence. This also matches the results seen in the voltage profile of the first cycle of the Na-APS hybrid battery cycled at 2 mA cm^{-2} current density (Fig. 4c), compared to the first cycle of the Na-APS hybrid battery cycled at 0.5 mA cm^{-2} (Fig. 4a). This further highlights the electrochemical participation of the anolyte at the Na metal anode and it is an area of interest for future work.

4. Conclusions

In summary, this work demonstrates, for the first time, a sodium-aqueous polysulfide (Na-APS) hybrid battery, in which a sodium-metal anode and the organic anolyte are protected from an aqueous polysulfide catholyte by means of a high ionic conductivity Na^+ ion solid electrolyte. The Na-APS hybrid battery displays good cyclability with the use of a freestanding CuS-CNT catalytic membrane that allows for cycling at high current densities with good rate performance. This work also demonstrates that unlike in a traditional room-temperature sodium-sulfur battery, care must be taken by appropriate choice of cycling parameters to avoid hydrogen evolution reaction and generation of H_2S gas in the aqueous catholyte. Future work to increase the ionic conductivity of the solid electrolyte can further reduce the battery overpotential, and improved microstructure can prevent Na dendrite growth through the ceramic grain boundaries to allow for ultra-long cycling lifetimes. Overall the Na-APS hybrid battery shows promise as a room-temperature sodium-sulfur battery system with long cycle life and high energy density.

Acknowledgements

This work was supported by the U.S. Department of Energy, Office of Basic Energy Sciences, Division of Materials Science and Engineering under Award No. DE-SC0005397.

Appendix A. Supplementary material

Supplementary data associated with this article can be found in the online version at (will be filled in by the editorial staff).

References

[1] M. Beaudin, H. Zareipour, A. Schellenberglabe, W. Rosehart. Energy storage for mitigating the variability of renewable electricity sources: An updated review. Energy Sustainable Dev. 14 (2010) 302-314.

[2] A. Chatzivasileiadi, E. Ampatzi, I. Knight. Characteristics of electrical energy storage technologies and their applications in buildings. Renewable Sustainable Energy Rev. 25 (2013) 814-830.

[3] J. B. Goodenough. Electrochemical energy storage in a sustainable modern society. Energy Environ. Sci. 7 (2014) 14-18.

[4] M. S. Dresselhaus, I. L. Thomas. Alternative energy technologies. Nature. 414 (2001) 332.

[5] P. Denholm, M. Hand. Grid flexibility and storage required to achieve very high penetration of variable renewable electricity. Energy Policy. 39 (2011) 1817-1830.

[6] D. Kumar, S. K. Rajouria, S. B. Kuhar, D. K. Kanchan. Progress and prospects of sodium-sulfur batteries: A review. Solid State Ionics. 312 (2017) 8-16.

[7] H. Kim, G. Jeong, Y.-U. Kim, J.-H. Kim, C.-M. Park, H.-J. Sohn. Metallic anodes for next generation secondary batteries. Chem. Soc. Rev. 42 (2013) 9011-9034.

[8] Z. Wen, J. Cao, Z. Gu, X. Xu, F. Zhang, Z. Lin. Research on sodium sulfur battery for energy storage. Solid State Ionics. 179 (2008) 1697-1701.

[9] J. K. Min, M. Stackpool, C. H. Shin, C.-H. Lee. Cell safety analysis of a molten sodium–sulfur battery under failure mode from a fracture in the solid electrolyte. J. Power Sources. 293 (2015) 835-845.

[10] K. B. Hueso, M. Armand, T. Rojo. High temperature sodium batteries: Status, challenges and future trends. Energy Environ. Sci. 6 (2013) 734-749.

[11] J. K. Min, C.-H. Lee. Numerical study on the thermal management system of a molten sodium-sulfur battery module. J. Power Sources. 210 (2012) 101-109.

[12] A. Manthiram, X. Yu. Ambient temperature sodium–sulfur batteries. Small. 11 (2015) 2108-2114.

[13] D. Kumar, S. B. Kuhar, D. K. Kanchan. Room temperature sodium-sulfur batteries as emerging energy source. J. Energy Storage. 18 (2018) 133-148.

[14] X. Yu, A. Manthiram. Room-temperature sodium–sulfur batteries with liquid-phase sodium polysulfide catholytes and binder-free multiwall carbon nanotube fabric electrodes. J. Phys. Chem. C. 118 (2014) 22952-22959.

[15] Y. X. Ren, H. R. Jiang, T. S. Zhao, L. Zeng, C. Xiong. Remedies of capacity fading in room-temperature sodium-sulfur batteries. J. Power Sources. 396 (2018) 304-313.

[16] Z. Qiang, Y.-M. Chen, Y. Xia, W. Liang, Y. Zhu, B. D. Vogt. Ultra-long cycle life, low-cost room temperature sodium-sulfur batteries enabled by highly doped (N, S) nanoporous carbons. Nano Energy. 32 (2017) 59-66.

[17] A. Kumar, A. Ghosh, A. Roy, M. R. Panda, M. Forsyth, D. R. MacFarlane, S. Mitra. High-energy density room temperature sodium-sulfur battery enabled by sodium polysulfide catholyte and carbon cloth current collector decorated with MnO_2 nanoarrays. Energy Storage Mater. (2018).

[18] Q. Lu, X. Wang, J. Cao, C. Chen, K. Chen, Z. Zhao, Z. Niu, J. Chen. Freestanding carbon fiber cloth/sulfur composites for flexible room-temperature sodium-sulfur batteries. Energy Storage Mater. 8 (2017) 77-84.

[19] R. D. Rauh, F. S. Shuker, J. M. Marston, S. B. Brummer. Formation of lithium polysulfides in aprotic media. J. Inorg. Nucl. Chem. 39 (1977) 1761-1766.

[20] L. Schafzahl, I. Hanzu, M. Wilkening, S. A. Freunberger. An electrolyte for reversible cycling of sodium metal and intercalation compounds. ChemSusChem. 10 (2017) 401-408.
[21] J. Lee, Y. Lee, J. Lee, S.-M. Lee, J.-H. Choi, H. Kim, M.-S. Kwon, K. Kang, K. T. Lee, N.-S. Choi. Ultraconcentrated sodium bis(fluorosulfonyl)imide-based electrolytes for high-performance sodium metal batteries. ACS Appl. Mater. Interfaces. 9 (2017) 3723-3732.
[22] G. Nikiforidis, M. C. M. van de Sanden, M. N. Tsampas, High and intermediate temperature sodium–sulfur batteries for energy storage: Development, challenges and perspectives. RSC Adv. 9 (2019) 5649-5673.
[23] S. Wenzel, H. Metelmann, C. Raiss, A. K. Durr, J. Janek, P. Adelhelm. Thermodynamics and cell chemistry of room temperature sodium/sulfur cells with liquid and liquid/solid electrolyte. J. Power Sources. 243 (2013) 758-765.
[24] I. Kim, J.-Y. Park, C. H. Kim, J.-W. Park, J.-P. Ahn, J.-H. Ahn, K.-W. Kim, H.-J. Ahn. A room temperature Na/S battery using a β″ alumina solid electrolyte separator, tetraethylene glycol dimethyl ether electrolyte, and a S/C composite cathode. J. Power Sources. 301 (2016) 332-337.
[25] L. Li, A. Manthiram. Decoupled bifunctional air electrodes for high-performance hybrid lithium-air batteries. Nano Energy. 9 (2014) 94-100.
[26] N. Li, Z. Weng, Y. Wang, F. Li, H.-M. Cheng, H. Zhou. An aqueous dissolved polysulfide cathode for lithium-sulfur batteries. Energy Environ. Sci. 7 (2014) 3307-3312.
[27] S. M. Hwang, W. Go, H. Yu, Y. Kim. Hybrid Na–air flow batteries using an acidic catholyte: Effect of the catholyte pH on the cell performance. J. Mater. Chem. A. 5 (2017) 11592-11600.
[28] L. Medenbach, P. Adelhelm, Cell concepts of metal–sulfur batteries (metal = Li, Na, K, Mg): Strategies for using sulfur in energy storage applications. Top. Curr. Chem. 375 (2017) 81.
[29] S. Licht. Aqueous solubilities, solubility products and standard oxidation-reduction potentials of metal sulfides. J. Electrochem. Soc. 135 (1988) 2971-2975.
[30] S. Licht. An energetic medium for electrochemical storage utilizing the high aqueous solubility of potassium polysulfide. J. Electrochem. Soc. 134 (1987) 2137-2141.
[31] P. M. Lessner, F. R. McLarnon, J. Winnick, E. J. Cairns. Aqueous polysulphide flow-through electrodes: Effects of electrocatalyst and electrolyte composition on performance. J. Appl. Electrochem. 22 (1992) 927-934.
[32] G. Hodes, J. Manassen. Electrocatalytic electrodes for the polysulfide redox system. J. Electrochem. Soc. 127 (1980) 544-549.
[33] M. S. Faber, M. A. Lukowski, Q. Ding, N. S. Kaiser, S. Jin. Earth-abundant metal pyrites (FeS_2, CoS_2, NiS_2, and their alloys) for highly efficient hydrogen evolution and polysulfide reduction electrocatalysis. J. Phys. Chem. C. 118 (2014) 21347-21356.
[34] G. Hodes, J. Manassen, D. Cahen. Photo-electrochemical energy conversion: Electrocatalytic sulphur electrodes. J. Appl. Electrochem. 7 (1977) 181-182.
[35] M. S. Faber, S. Jin. Earth-abundant inorganic electrocatalysts and their nanostructures for energy conversion applications. Energy Environ. Sci. 7 (2014) 3519-3542.
[36] P. Han, S.-H. Chung, A. Manthiram. Thin-layered molybdenum disulfide nanoparticles as an effective polysulfide mediator in lithium–sulfur batteries. ACS Appl. Mater. Interfaces. 10 (2018) 23122-23130.
[37] P. T. Dirlam, J. Park, A. G. Simmonds, K. Domanik, C. B. Arrington, J. L. Schaefer, V. P. Oleshko, T. S. Kleine, K. Char, R. S. Glass, C. L. Soles, C. Kim, N. Pinna, Y.-E. Sung, J.

Pyun. Elemental sulfur and molybdenum disulfide composites for Li–S batteries with long cycle life and high-rate capability. ACS Appl. Mater. Interfaces. 8 (2016) 13437-13448.
[38] T. A. Bendikov, C. Yarnitsky, S. Licht. Energetics of a zinc-sulfur fuel cell. J. Mater. Chem. B. 106 (2002) 2989-2995.
[39] D. Peramunage, S. Licht. A solid sulfur cathode for aqueous batteries. Science. 261 (1993) 1029-1032.
[40] M. M. Gross, A. Manthiram. Aqueous polysulfide–air battery with a mediator-ion solid electrolyte and a copper sulfide catalyst for polysulfide redox. ACS Appl. Energy Mater. (2018).
[41] Z. Yao, X. Zhu, C. Wu, X. Zhang, Y. Xie. Fabrication of micrometer-scaled hierarchical tubular structures of CuS assembled by nanoflake-built microspheres using an in situ formed Cu(I) complex as a self-sacrificed template. Cryst. Growth Des. 7 (2007) 1256-1261.
[42] L. Li, X. Zhao, A. Manthiram. A dual-electrolyte rechargeable Li-air battery with phosphate buffer catholyte. Electrochem. Commun. 14 (2012) 78-81.
[43] M. M. Gross, A. Manthiram. Rechargeable zinc-aqueous polysulfide battery with a mediator-ion solid electrolyte. ACS Appl. Mater. Interfaces. 10 (2018) 10612-10617.
[44] A. Rudola, D. Aurbach, P. Balaya. A new phenomenon in sodium batteries: Voltage step due to solvent interaction. Electrochem. Commun.. 46 (2014) 56-59.
[45] S. H. Ge, B. Yi, H. Zhang. Study of a high power density sodium polysulfide/bromine energy storage cell. J. Appl. Electrochem. 34 (2004) 181-185.
[46] Z. Li, M. Sam Pan, L. Su, P.-C. Tsai, A. F. Badel, J. M. Valle, S. L. Eiler, K. Xiang, F. R. Brushett, Y.-M. Chiang. Air-breathing aqueous sulfur flow battery for ultralow-cost long-duration electrical storage. Joule. 1 (2017) 306-327.
[47] R. Demir-Cakan, M. Morcrette, J.-M. Tarascon. Use of ion-selective polymer membranes for an aqueous electrolyte rechargeable Li-ion–polysulphide battery. J. Mater. Chem. A. 3 (2015) 2869-2875.

Figure Captions

Fig. 1 Schematic of a sodium-aqueous polysulfide hybrid battery with a sodium-metal anode, organic anolyte, Na^+-ion conducting solid-electrolyte separator, and an alkaline aqueous polysulfide catholyte.

Fig. 2 Characterization of the freestanding CuS-CNT electrode. (a) Schematic of the CuS-CNT electrode preparation. (b) SEM and EDS maps of the CuS-CNT electrode. High resolution SEM images of the (c) CuS microtube, (d) CuS nanoflowers, and (e) interwoven CNT. (f) XRD pattern of the CuS-CNT electrode.

Fig. 3 Cyclic voltammetry of Na-APS hybrid batteries with 0.1 M Na_2S_4 + 1 mM NaOH catholyte and CNT electrodes at a scan rate of 0.1 mV s^{-1} at (a) 1.2 – 2.8 V and (b) 1.8 – 2.8 V. (c) Single discharge-charge cycle of a Na-APS hybrid battery with 1 M $NaClO_4$ in EC : PC + 5% FEC anolyte, and (d) initial discharge of a Na-APS battery with different anolytes.

Fig. 4 Galvanostatic cycling performance of the Na-APS hybrid battery: (a) voltage profile, and (b) energy density and energy efficiency at 0.5 mA cm^{-2} current density; (c) voltage profile and (d) energy density and energy efficiency at 2 mA cm^{-2} current density.

Fig. 5 Rate performance of the Na-APS hybrid battery (a) with CNT electrode and (b) with CuS-CNT electrode. (c) Evolution of the Na-APS hybrid battery discharge curves with increasing current density.

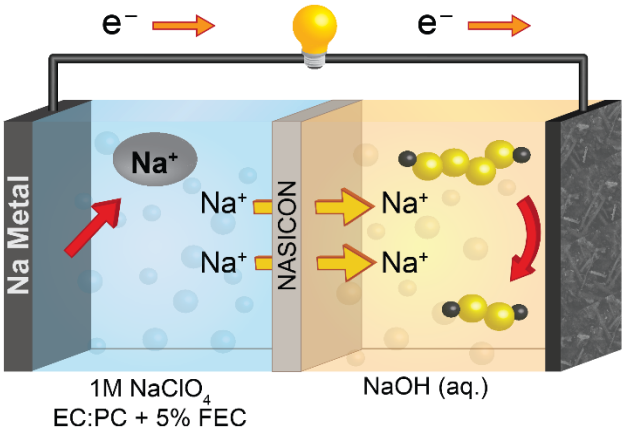

Fig. 1 Schematic of a sodium-aqueous polysulfide hybrid battery with a sodium-metal anode, organic anolyte, Na^+-ion conducting solid-electrolyte separator, and an alkaline aqueous polysulfide catholyte.

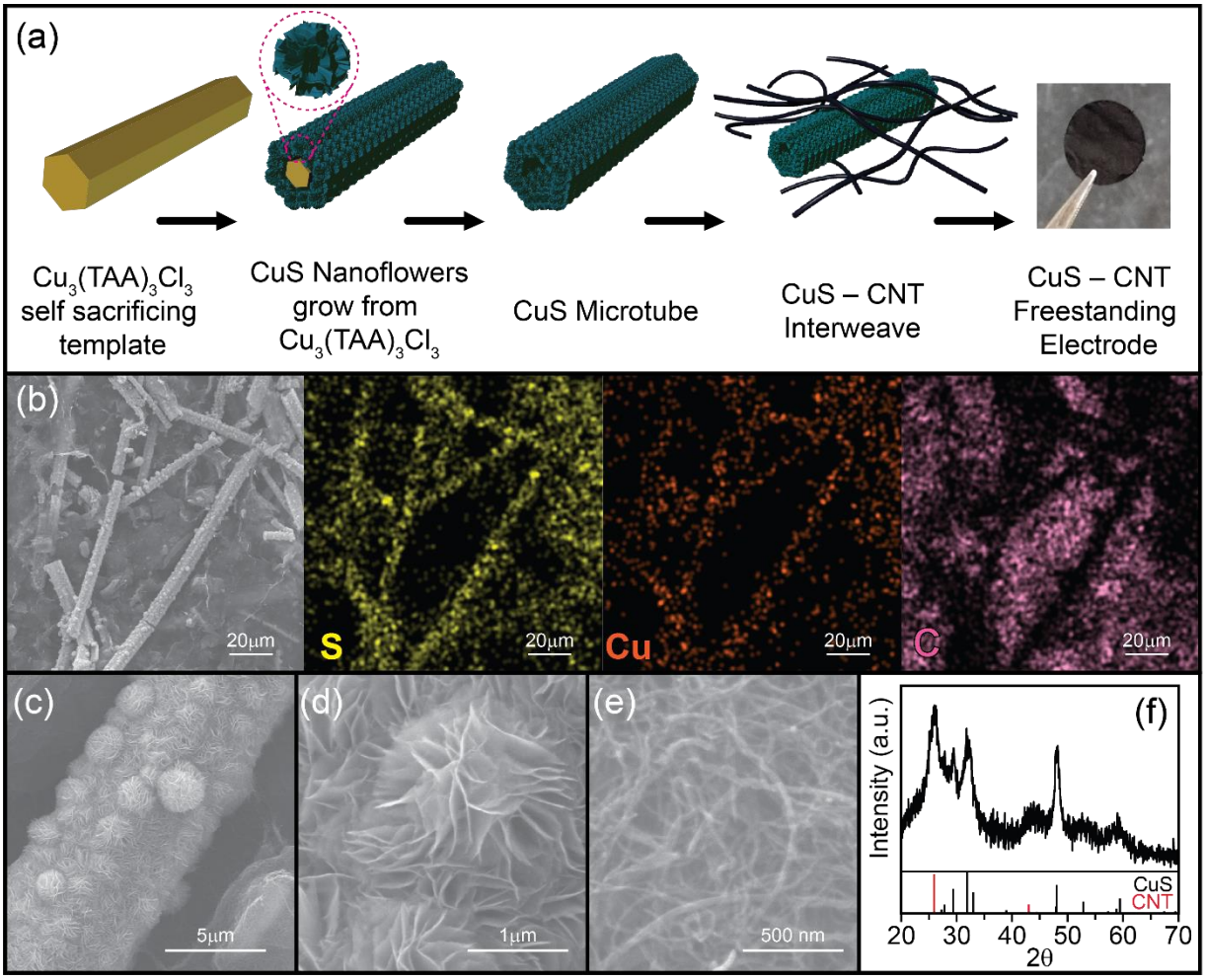

Fig. 2 Characterization of the freestanding CuS-CNT electrode. (a) Schematic of the CuS-CNT electrode preparation. (b) SEM and EDS maps of the CuS-CNT electrode. High resolution SEM images of the (c) CuS microtube, (d) CuS nanoflowers, and (e) interwoven CNT. (f) XRD pattern of the CuS-CNT electrode.

.

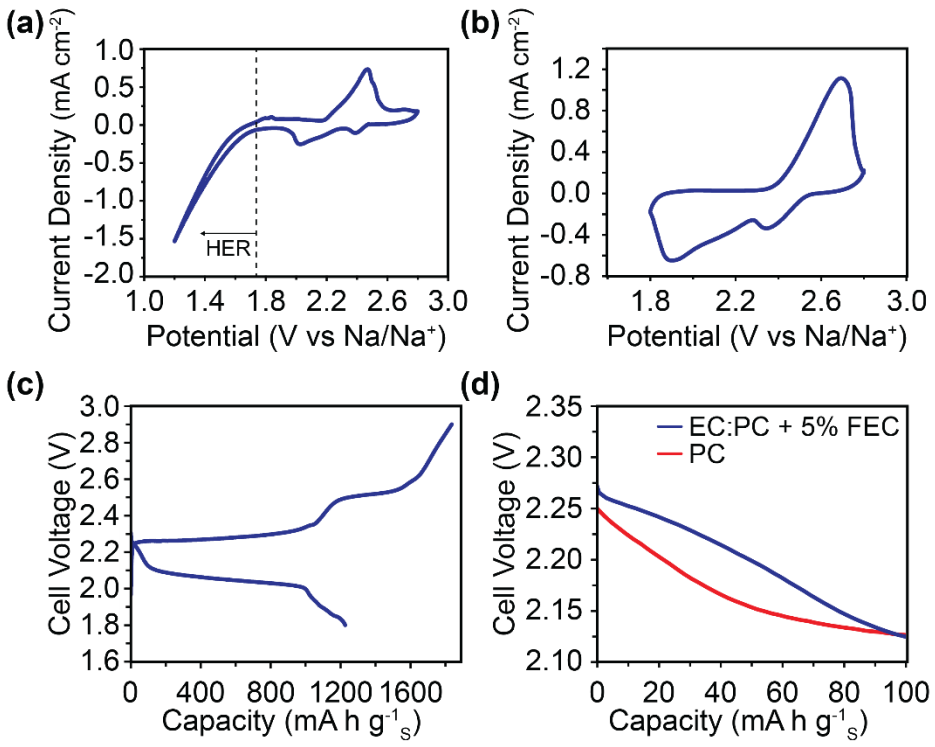

Fig. 3 Cyclic voltammetry of Na-APS hybrid batteries with 0.1 M Na_2S_4 + 1 mM NaOH catholyte and CNT electrodes at a scan rate of 0.1 mV s^{-1} at (a) 1.2 – 2.8 V and (b) 1.8 – 2.8 V. (c) Single discharge-charge cycle of a Na-APS hybrid battery with 1 M $NaClO_4$ in EC : PC + 5% FEC anolyte, and (d) initial discharge of a Na-APS battery with different anolytes.

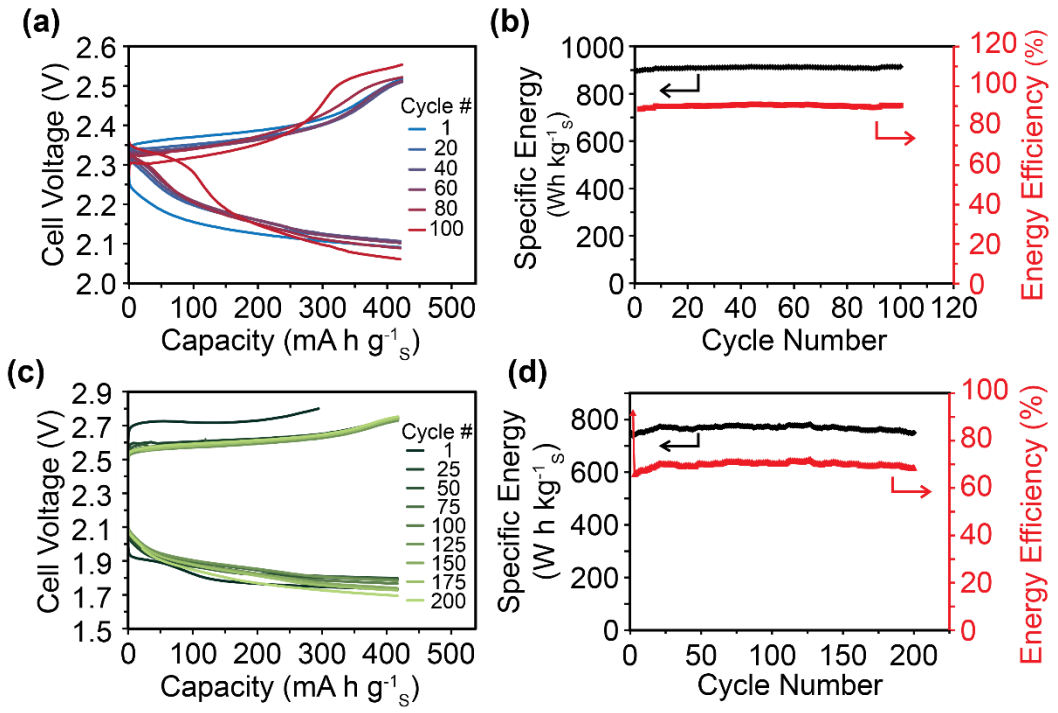

Fig. 4 Galvanostatic cycling performance of the Na-APS hybrid battery: (a) voltage profile, and (b) energy density and energy efficiency at 0.5 mA cm^{-2} current density; (c) voltage profile and (d) energy density and energy efficiency at 2 mA cm^{-2} current density.

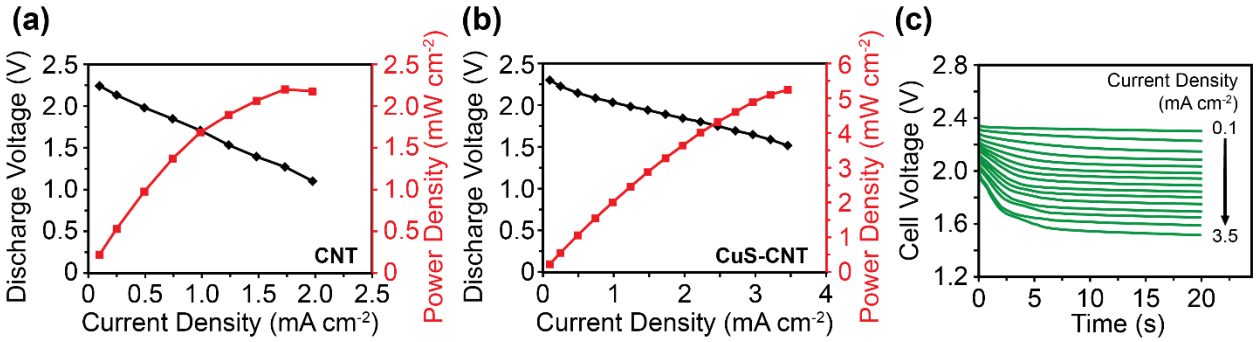

Fig. 5 Rate performance of the Na-APS hybrid battery (a) with CNT electrode and (b) with CuS-CNT electrode. (c) Evolution of the Na-APS hybrid battery discharge curves with increasing current density.